Novel rare earth metal and aluminium codoped ZnO photocatalysts for degradation of rhodamine b dye

M. S. Viswaksenan[a], A. Simi[b,*], A. Panneerselvam[c]
[a]*Reserch Scholar, Bharathidasan university, Trichirapalli-620 002, Tamilnadu, India*
[b]*St. Josephs college (Autonomous), Trichirapalli-620002, Tamilnadu, India*
[c]*Vivekanandha college of Engineering for women, Tiruchengode-637205, Tamilnadu, India*

In this study, samarium and aluminium codoped zinc oxide nanostructures were produced via a soft chemical route, and their structural, morphological, optical, and photocatalytic capabilities were investigated. X-ray diffraction (XRD) patterns and photoluminescence (PL) studies show that both undoped and Sm & Al codoped ZnO nanostructures have a hexagonal wurtzite crystal structure. The shape of the sample's hexagonal nanostructures, as seen in FESEM pictures, changes as the amount of Sm^{3+} doping increases. Sm^{3+} and Al^{2+} ions have been incorporated into ZnO, as seen by the EDX spectra. ZnO nanostructures were thoroughly studied to learn how Al^{2+} and Sm^{3+} doping affected their structure, shape, absorption, emission, and photocatalytic activity. The capacity to absorb visible light is enhanced by the incorporation of Sm^{3+} ions, which causes a red shift in the optical energy band gap from 2.5 to 3.2 eV. Based on the results of in-depth photocatalytic tests, it has been shown that Sm & Al codoped ZnO nanostructures exhibit the highest photodegradation efficiency for RhB dye for $Sm_{0.04M}Al_{0.04M}Zn_{0.92M}O$, i.e. 84%, when exposed to visible light. ZnO, when doped with a rare earth metal ion (Sm^{3+}), displays enhanced photocatalytic efficiency and might have real-world uses. In this research, nanoscale photocatalysts, as manufactured, degrade RhB dye effectively as a photocatalyst.

(Received March 31, 2023; Accepted July 18, 2023)

Keywords: RhB, Sm, Al, ZnO, Photocatalyst

1. Introduction

It is possible that the quality of the environment would deteriorate as a result of the wastewater effluents generated by sectors such as food processing and mining [1, 2]. The textile dyeing business is one of the major users of water and dischargers of wastewater. This makes the industry one of the most water-intensive industries [3]. These effluents carry a wide variety of pollutants, including acids, alkalis, dyes, surfactants, and both organic and inorganic waste products. Rhodamine B, sometimes known as RhB, is a popular nitrogen-containing dye that is used in industry. To alter the metal oxide, four gemini surfactants, each with a distinct functional group (imino, hydroxyl, phenyl, and pyridyl), were created [4]. It was anticipated that the resultant would have a better adsorption capacity owing to a variety of hydrogen bond and interactions. To this day, efforts have been made to reduce the amount of dye pollution in water using a variety of different approaches. This category includes a wide range of methods, including chemical, photochemical, biological, and physical techniques. The use of photodegradation as a removal technique offers a number of advantages when it comes to the cleansing of wastewater. In recent years, there has been a lot of interest in the use of oxide nanoparticles for the removal of organic dyes. This is due to the fact that oxide nanoparticles have the capacity to undergo photocatalytic destruction of organic hazardous pollutants [5, 6]. As a potential method for cleaning wastewater, photocatalysts constructed from metal oxide semiconductors show a great deal of promise. This is because to how simple it is to produce them, requiring just moderate reaction conditions and a

* Corresponding author: simisjc82@gmail.com
https://doi.org/10.15251/DJNB.2023.183.859

little amount of relatively inexpensive energy. For example, semiconducting materials based on zinc oxide (ZnO), which has applications in a wide range of different sectors, have been the focus of a significant amount of study in recent years (photocatalysis). In recent years, research has shown that the photocatalytic activity of samarium-doped materials has significantly improved [7,8]. It has been observed that the photo degradation capabilities of ZnO that has been doped with rare-earth (RE) cations such as La, Sm, Eu, and Ce are greatly increased. It is important to notice the influence that doping with rare earth elements has on ZnO's characteristics [9]. It has been discovered that even minute amounts of bulky rare earth cations may have a significant influence on the structural properties, crystallite sizes, surface defects, and, ultimately, the photocatalytic capabilities of the host material. The hydrothermal approach, the sol gel method, the coprecipitation method, and the micro-emulsion templating method are the most popular ways that inorganic oxide nanomaterials may be generated[10,11]. To create doped metal oxide nanostructured materials with improved specific surface areas and enhanced photocatalytic capabilities, the soft chemical approach was used in this research as a flexible and straightforward process. This method was chosen because of its simplicity[12]. At this point, a number of research have focused on the soft chemical method for the synthesis of doped metal oxides. The codoping of zinc oxide with Al and Sm has been accomplished using this approach with great effectiveness. Despite this, there were very few research that looked at the possibility of using doped ZnO for the photodegradation of RhB dyes. Recent work by Naseri[13] and colleagues has resulted in the fabrication of ZnO/CuO nanofibers with varying concentrations of CuO. Throughout the course of their research, the photocatalytic degradation of methylene blue was investigated, and the researchers discovered that this particular kind of catalyst had the potential to hold great promise for the efficient removal of certain organic contaminants from waterways. Moreover, it was established that a greater catalytic performance may be produced in ZnO/CuO nanofibers by adjusting the amount of CuO that is present in the nanofibers. Zheng[14] and his co-authors examined the photocatalytic activity of Rhodamine B's breakdown when it was exposed to UV light. In this particular application, the scientists made use of La-doped ZnO/C fibrous catalytic materials having a core–shell structure. These materials were generated by the calcination of $La(NO)_3/Zn(Ac)_2$ composite nanofibers. In this present work, using soft chemical methods, create unique nanostructured materials that were based on zinc oxide that had been doped with aluminium and a rare-earth element (Sm). In addition, the development of various concentrations of ZnO/Sm/Al nanostructures by soft chemical method and then their testing for dye degradation have not been reported in the literature up until this point. This is despite the fact that we have done both of these things. In addition, the newly created materials have been studied in terms of their surface morphology, crystalline structure, and optical characteristics. In terms of applications, the removal of RhB dye from synthetic wastewaters in the presence of these materials received the majority of the attention and focus.

2. Experimental work

2.1. Preparation of samarium and Aluminium codoped ZnO NPs

Individually, 0.98M zinc nitrate, 0.01M samarium nitrate hexahydrate, and 0.01M aluminium nonahydrate were diluted in 100 cc of distilled water while rapidly whirling the solution. The main mixture was then poured drop-by-drop to 25 mL of 2M NaOH while the container was continuously agitated. Continuous stirring of the mixture causes the formation of a white precipitate. After separating the precipitate from the remainder of the mixture, it was repeatedly washed in double-distilled water and ethanol. The final piece was then annealed for three hours at 450 degrees and dried for one hour at 100 degrees in the oven. The obtained nanoparticles were ground into powder, and the jar holding the powder was placed away for safety. Whether we were dealing with $Sm_{0.02}Al_{0.02}Zn_{0.96}O$, $Sm_{0.03}Al_{0.03}Zn_{0.94}O$, or $Sm_{0.04}Al_{0.04}Zn_{0.92}O$, the method was same. Zinc nitrate at a concentration of 0.1M and sodium hydroxide at a concentration of 2.0M were used to create undoped ZnO NPs.

2.2. Photocatalytic measurements

Nanocatalysts with and without Sm and Al doping had their photocatalytic activities measured in a photocatalytic reactor. RhB dye degradation under visible light irradiation was

tested using the produced materials as photocatalysts. Dye photodegradation was carried out using an effective photocatalyst in a photocatalytic reactor. A photocatalytic reactor, complete with quartz double jacket tube, water circulating unit, magnetic stirrer, and air supply opening, was used to conduct the analysis. The reactor consisted of a quartz double jacket tube with visible light(300W) put in the middle, with water circulating continuously around the outer tube. In order to keep the lamp from getting too hot, a circulating unit supplied constant flows of cold water. The PID controller for temperature allowed for constant monitoring. There is a timer so that we can determine how much time has passed after the samples were exposed to radiation. In order to measure the efficiency of photo degradation, a constant amount of photocatalyst was taken and distributed in a dye solution for a constant period of time. Analysis of the degradation of an aqueous solution of RhB dye was used to compare the photocatalytic activities of the obtained undoped and codoped ZnO nanocatalysts[15,16].

3. Result and discussion

3.1. XRD analysis

Figure 1 depicts the X-ray diffraction patterns of the nanocatalysts $Sm_{0.01M}Al_{0.01M}Zn_{0.98M}O$, $Sm_{0.02M}Al_{0.02M}Zn_{0.96M}O$, $Sm_{0.03M}Al_{0.03M}Zn_{0.94M}O$, and $Sm_{0.04M}Al_{0.04M}Zn_{0.92M}O$. Undoped ZnO catalyst has a strong intensity peak at 34.57°, corresponding to the (002) plane, and low intensity peaks at 31.68°, 36.26°, 47.75°, and 62.76°, corresponding to the (100), (101), (102) and (103) planes, respectively. The existence of these planes suggests that only a ZnO phase with a hexagonal crystal structure may develop (JCPDS file number: 890510). In addition, the addition of Sm and Al as a doping element abruptly lowered the strength of the dominating peak (002) because the c-axis orientation was reduced in proportion to Sm and Al concentration. Nevertheless, in the other two main planes, (100) and (101), peak intensity increased with increasing Sm and Al doping concentrations. This may be a result of the transition of the c-axis orientation from (002) to (100) and (101), respectively (101). Furthermore, the c-axis orientation of the (100) plane was greater than that of the (101) plane. This means that, for the (100) plane, the c-axis orientations of the grains become equally perpendicular to the substrate surface. Synthesized nanocatalysts exhibited no further peaks. This indicates that the introduction of Sm ions into the hexagonal structure of ZnO resulted in an expansion of the ZnO lattice along the c-axis and a contraction along the a-axis in order to maintain the Wurtzite structure of ZnO. To determine the average crystallite size of synthesised NPs, the Scherrer equation (1) was used[17].

$$D=K\lambda / (\beta \cos \theta) \quad (1)$$

When the crystals were calculated, their average nanosizes were 40.07, 37.45, 35.25, 37.61, and 38.7 nm. Due to the integration of Sm^{2+} and Al^{3+} into the ZnO matrix, the size of ZnO crystallites doped with Sm and Al decreased. In contrast, the increased size of Sm, Al-codoped ZnO NPs was ascribed to a significant number of defects caused by the higher concentration of Sm^{2+} ions in the Al-ZnO matrix.

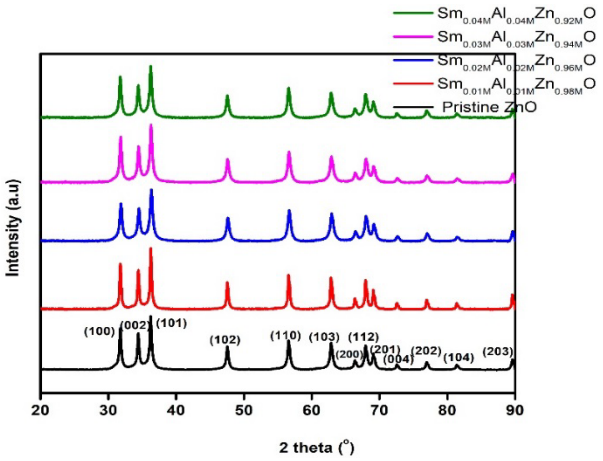

Fig. 1. XRD pattern of pure, $Sm_{0.01M}Al_{0.01M}Zn_{0.98M}O$, $Sm_{0.02M}Al_{0.02M}Zn_{0.96M}O$, $Sm_{0.03M}Al_{0.03M}Zn_{0.94M}O$, and $Sm_{0.04M}Al_{0.04M}Zn_{0.92M}O$.

3.2. FTIR analysis

The functional groups included in the synthesised nanocrystals of heterogeneous metal oxides were identified using FTIR spectroscopy. These particles were made up of a combination of pure ZnO and ZnO NPs doped with various concentrations of Sm and Al. The bandwidth of the metal oxide nanoparticles' fingerprint area was found to be 544 cm^{-1}. The symmetric vibrations of the C=O molecule is shown by the prominent peak at 1592 cm^{-1}. The existence of -OH bending and stretching vibration peaks can be seen in the FTIR spectra at 845 cm^{-1} and 3774 cm^{-1}. The bandwidth of the metal oxide nanoparticles' fingerprint area was found to be 544 cm^{-1}. The symmetrical vibration within the C=O molecules is shown by the prominent peak at 1592 cm^{-1}. This is owing to the vibration of the Sm, Al, and Zn-O bonds, which was seen as a peak at 845 cm^{-1} over an extensive range of Sm/Al codoped ZnO concentration. This is because ZnO may be treated with varying amounts of Sm and Al. Variable amounts of Sm and Al particles in the ZnO matrix are shown decisively by changes in peak shifts. These distinctions are obvious at the top. When two dopants in it Sm and Al, are introduced to ZnO, mixed metal oxides arise. This process causes substances to be substituted for Zn elements in the crystal structure, resulted in the production of heterogeneous metal oxides[18].

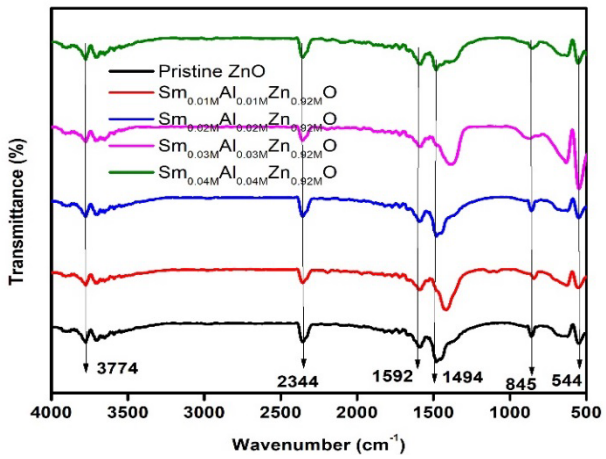

Fig. 2. FTIR analysis of pure, $Sm_{0.01M}Al_{0.01M}Zn_{0.98M}O$, $Sm_{0.02M}Al_{0.02M}Zn_{0.96M}O$, $Sm_{0.03M}Al_{0.03M}Zn_{0.94M}O$, and $Sm_{0.04M}Al_{0.04M}Zn_{0.92M}O$.

3.3. SEM/EDAX analysis

Figure 3 shows SEM and EDAX images of pure, $Sm_{0.01M}Al_{0.01M}Zn_{0.98M}O$, $Sm_{0.02M}Al_{0.02M}Zn_{0.96M}O$, $Sm_{0.03M}Al_{0.03M}Zn_{0.94M}O$, and $Sm_{0.04M}Al_{0.04M}Zn_{0.92M}O$. On the ZnO surface, Zinc, Oxygen, Aluminum, and Samarium are evenly dispersed. Figure 3(b, d, f, and g) shows the EDAX spectrum of nanoparticles that have been produced. The film is stoichiometric and contains no additional chemical species. Elements of Zinc, Oxygen, Aluminum, and Samarium are detected in the film[19].

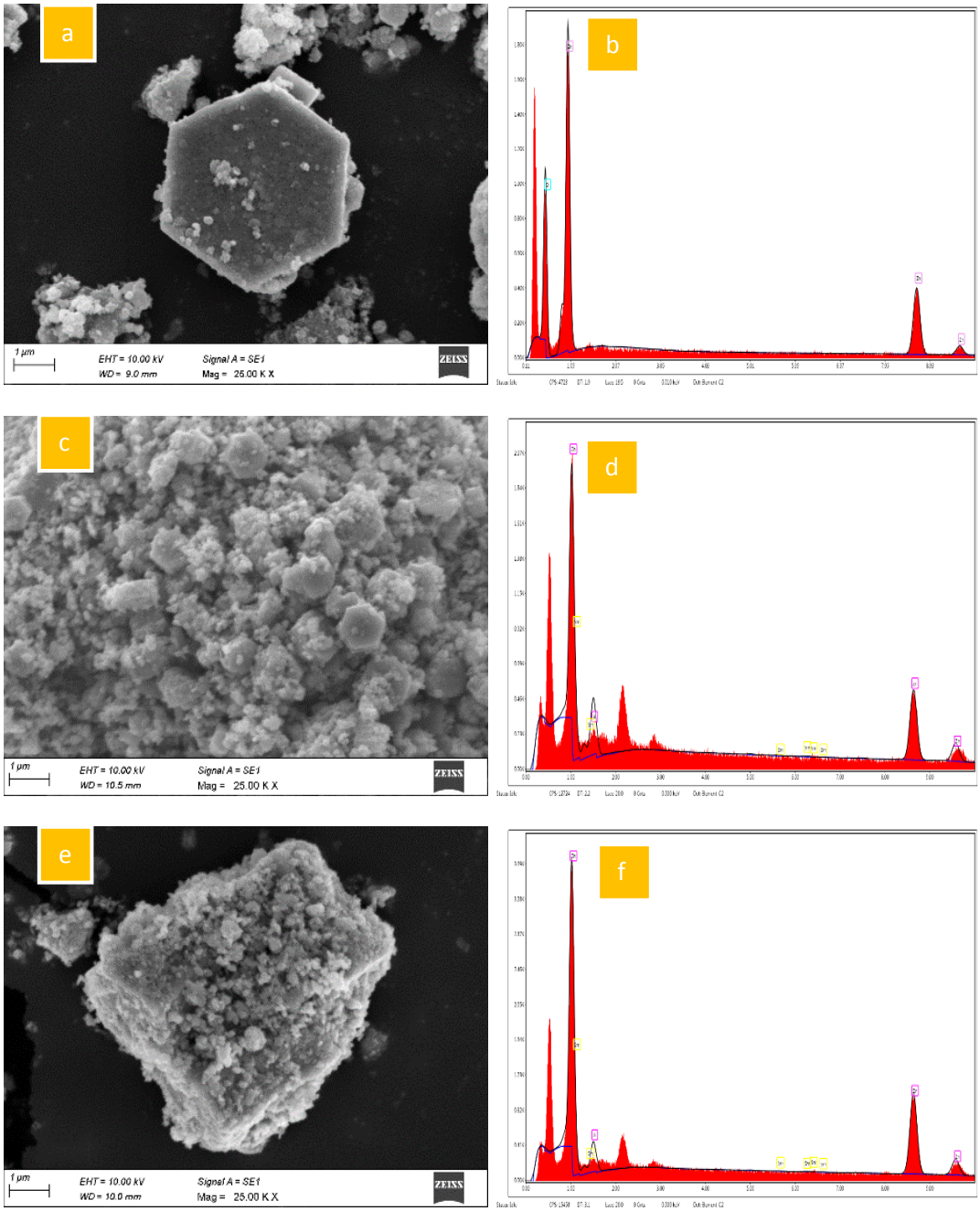

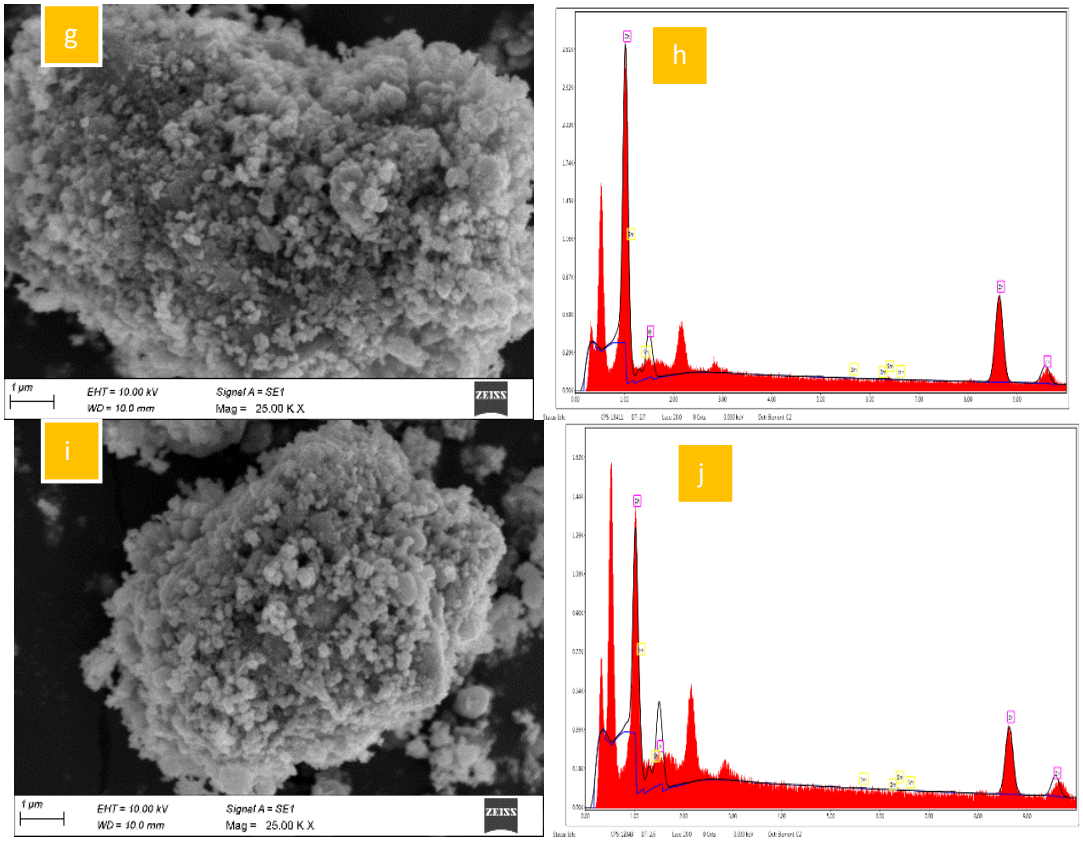

Fig. 3. SEM and EDAX analysis of pure, $Sm_{0.01M}Al_{0.01M}Zn_{0.98M}O$, $Sm_{0.02M}Al_{0.02M}Zn_{0.96M}O$, $Sm_{0.03M}Al_{0.03M}Zn_{0.94M}O$, and $Sm_{0.04M}Al_{0.04M}Zn_{0.92M}O$.

3.4. Ultraviolet-visible spectroscopy and bandgap calculation

Using ultraviolet spectroscopy, the UV spectra of pure and $Sm_{0.01M}Al_{0.01M}Zn_{0.98M}O$, $Sm_{0.02M}Al_{0.02M}Zn_{0.96M}O$, $Sm_{0.03M}Al_{0.03M}Zn_{0.94M}O$, and $Sm_{0.04M}Al_{0.04M}Zn_{0.92M}O$ nanocatalysts were determined (Figure 3). Comparing the spectra of ZnO nanoparticles doped with Sm and Al to those of pure ZnO reveals that the presence of these ions causes a red shift in the absorption edge at shorter wavelengths. This is evident when comparing the spectra of the two groups. Maximum absorbance values for pure ZnO and different concentrations of Sm and Al codoped ZnO NPs are 344, 389, 391, 393, and 391, respectively. When Al^{3+} and Sm^{2+} ions are injected into ZnO NPs, the intensities of the peaks resulting from the various ratios of Sm, Al-ZnO NPs are altered. Using the equation (2)

$$(hv)n = A(hv-Eg) \quad (2)$$

The bandgap (figure 5) of pure ZnO and Sm, Al-doped ZnO NPs was found to be 3.2, 3.1, 2.9, 2.7, and 2.5 eV, respectively. Due to the increased concentration of Sm^{2+} ions in the ZnO system, the Sm, Al-doped ZnO NPs exhibited a smaller band gap. According to the previously given perspectives, Sm^{2+} ions and Al^{3+} are effectively integrated into the ZnO lattice.

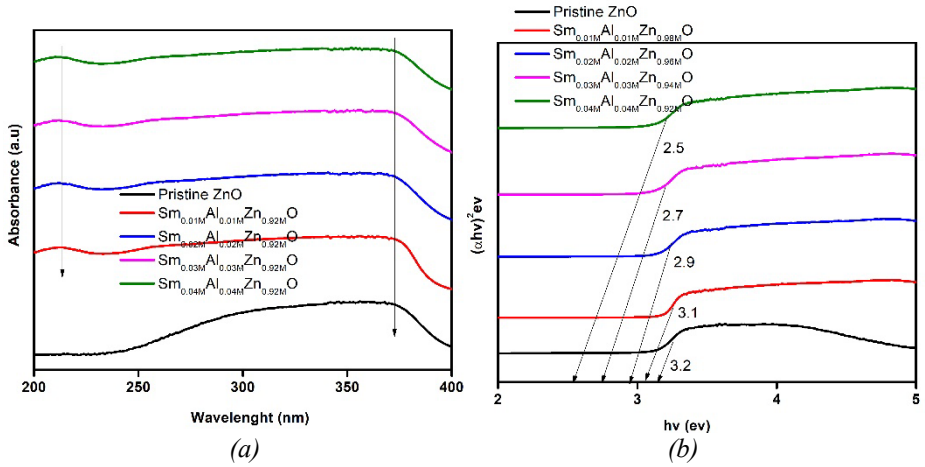

Fig. 4. (a) Uv-Vis and (b) Bandgap analysis of pure, $Sm_{0.01M}Al_{0.01M}Zn_{0.98M}O$, $Sm_{0.02M}Al_{0.02M}Zn_{0.96M}O$, $Sm_{0.03M}Al_{0.03M}Zn_{0.94M}O$, and $Sm_{0.04M}Al_{0.04M}Zn_{0.92M}O$.

3.5. Photoluminescence analysis

Figure 6 displays the photoluminescence spectra of pure and $Sm_{0.01M}Al_{0.01M}Zn_{0.98M}O$, $Sm_{0.02M}Al_{0.02M}Zn_{0.96M}O$, $Sm_{0.03M}Al_{0.03M}Zn_{0.94M}O$, and $Sm_{0.04M}Al_{0.04M}Zn_{0.92M}O$ at room temperature. The spectrum exhibits peaks akin to the luminescence spectra of pure ZnO nanoparticles. The first two peaks, situated at about 480 nm and 490 nm, are the result of recombination between e^-_{CB} and h^+_{VB}, while the peaks placed at approximately 470 nm and 450 nm are the result of recombination between e^-_{CB} and h^+_{VB}. The intensity shift indicates that Sm^{2+} and Al^{3+} have been introduced into the ZnO system, and the broad peaks indicate that the synthesised Sm, Al-doped ZnO nanoparticles have less flaws.

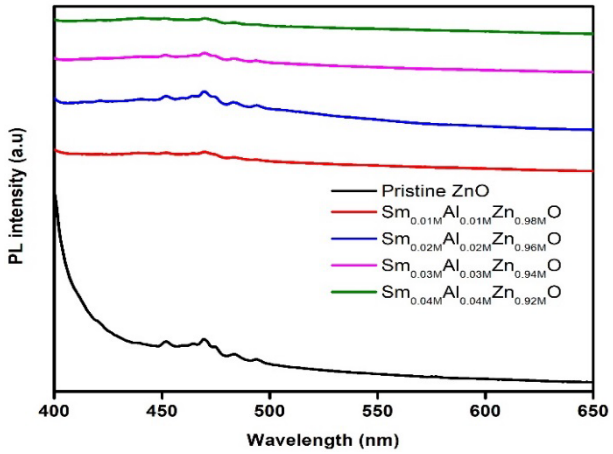

Fig. 5. PL spectra analysis of pure, $Sm_{0.01M}Al_{0.01M}Zn_{0.98M}O$, $Sm_{0.02M}Al_{0.02M}Zn_{0.96M}O$, $Sm_{0.03M}Al_{0.03M}Zn_{0.94M}O$, and $Sm_{0.04M}Al_{0.04M}Zn_{0.92M}O$ nanocatalyst.

3.6. Photodegradation efficiency

Figure 6 illustrates the UV-vis absorption spectra of RhB dye solution over pure, $Sm_{0.01M}Al_{0.01M}Zn_{0.98M}O$, $Sm_{0.02M}Al_{0.02M}Zn_{0.96M}O$, $Sm_{0.03M}Al_{0.03M}Zn_{0.94M}O$, and $Sm_{0.04M}Al_{0.04M}Zn_{0.92M}O$ nanocatalyst. It is evident that the strength of RhB's absorption peaks reduces as irradiation duration increases, showing the dye's elimination. Significantly, the absorbance of RhB quickly decreases in the presence of the produced catalyst, and the absorbance is almost linear after 60 minutes of illumination. 51%, 55%, 64%, 71%, and 84% were the

photocatalytic efficiencies of synthesized nanocatalysts, respectively. Due to the increase in crystallinity, the photocatalytic effectiveness of synthesised NPs steadily improves. The remarkable photocatalytic degradation efficiency of 84% of $Sm_{0.04M}Al_{0.04M}Zn_{0.92M}O$ nanoparticles calcined at 450°C is attributable to their better crystallinity and specific surface area, which provide more active sites for photocatalytic reaction. In addition, the structure of the nanoparticles might offer an effective channel for charge transfer and minimise the combination of photogenerated electron-hole pairs, hence promoting the enhancement of degrading efficiency.

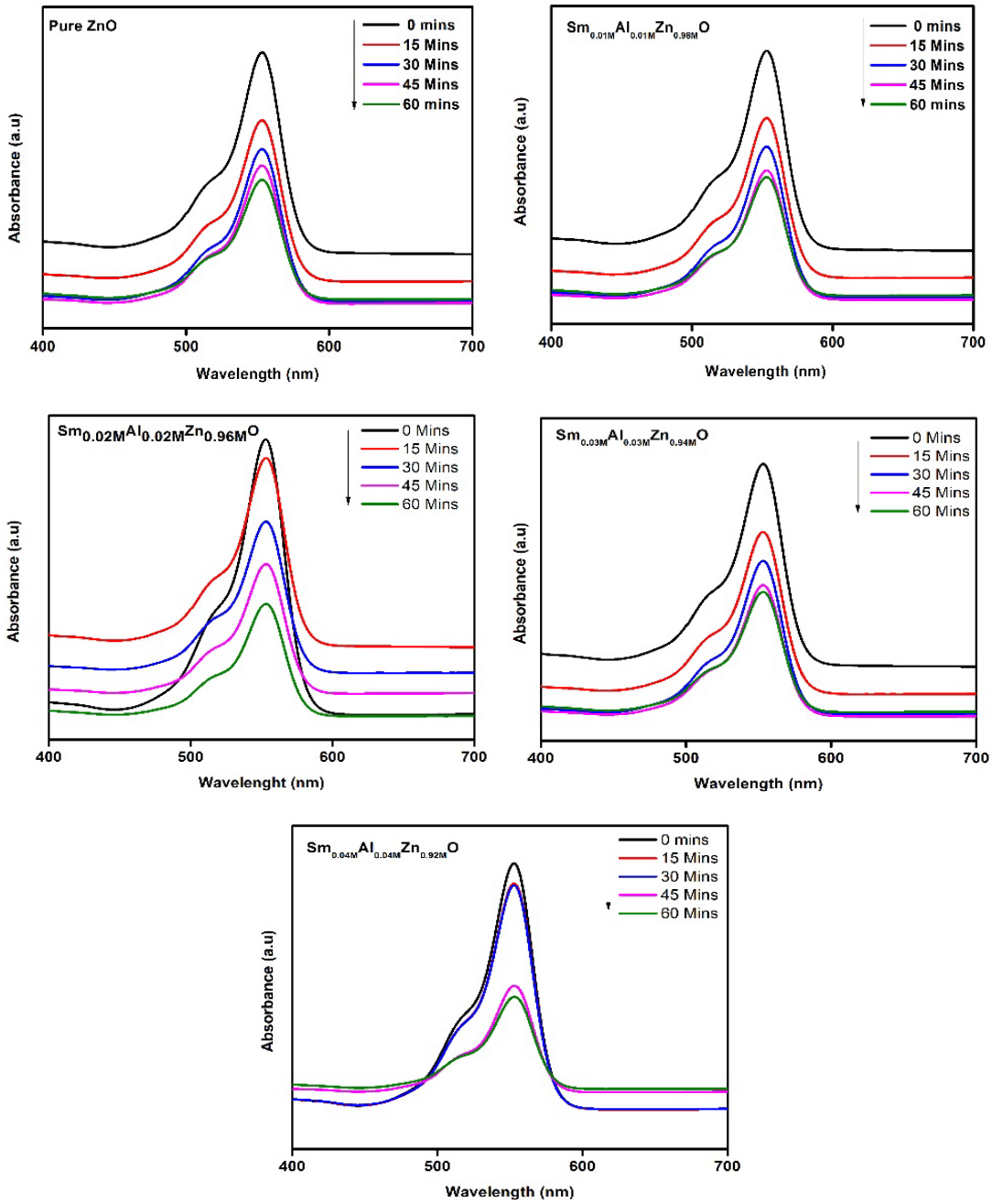

Fig. 6. Photodegradation Efficiency of pure, $Sm_{0.01M}Al_{0.01M}Zn_{0.98M}O$, $Sm_{0.02M}Al_{0.02M}Zn_{0.96M}O$, $Sm_{0.03M}Al_{0.03M}Zn_{0.94M}O$, and $Sm_{0.04M}Al_{0.04M}Zn_{0.92M}O$ nanocatalyst.

4. Conclusion

In short, the soft chemical method was used to make pure, $Sm_{0.01M}Al_{0.01M}Zn_{0.98M}O$, $Sm_{0.02M}Al_{0.02M}Zn_{0.96M}O$, $Sm_{0.03M}Al_{0.03M}Zn_{0.94M}O$, and $Sm_{0.04M}Al_{0.04M}Zn_{0.92M}O$ nanocatalysts. In this report, we use a soft chemical method to make a rare earth co-doped AlZnO nanocatalyst. Samarium (Sm^{3+}) and aluminium (Al^{3+}) are successfully spread out and mixed into the ZnO lattice, respectively. Structure, optical, Photoluminescence, and FTIR studies were done on the samples that were taken. The structures in an XRD spectrum look like hexagons. By increasing the Sm and Al concentrations, the Crystalline gets better. They are good for optoelectronic applications because they have good optical and PL properties. The fingerprint region of metal oxide nanoparticles has a bandwidth of 716.17 cm^{-1}, with a large peak at 3723 cm^{-1} corresponding to the Zn-O bond stretching vibration and a sharp peak at 1531 cm^{-1} corresponding to the OH bond stretching vibration. The samples have band gaps of about 3.2, 3.1, 2.9, 2.7, and 2.5 eV, which also proves that Sm and Al ions exist. Samples also exhibit excellent photoluminescence behaviour. The PL spectrum shows peaks at 480 nm and 490 nm, and the strength of the peaks increases with the amount of Sm and Al in the starting solution. Photocatalytic activity leads to degradation at rates of 51%, 55%, 64%, 71%, and 84% for pure, $Sm_{0.01M}Al_{0.01M}Zn_{0.98M}O$, $Sm_{0.02M}Al_{0.02M}Zn_{0.96M}O$, $Sm_{0.03M}Al_{0.03M}Zn_{0.94M}O$, and $Sm_{0.04M}Al_{0.04M}Zn_{0.92M}O$ nanocatalysts.

References

[1] Ilyas, Muhammad, Waqas Ahmad, Hizbullah Khan, Saeeda Yousaf, Muhammad Yasir, and Anwarzeb Khan, Reviews on environmental health 34, no. 2 (2019): 171-186; https://doi.org/10.1515/reveh-2018-0078

[2] Ahmad, Talha, Rana Muhammad Aadil, Haassan Ahmed, Ubaid ur Rahman, Bruna CV Soares, Simone LQ Souza, Tatiana C. Pimentel et al., Trends in Food Science & Technology 88 (2019): 361-372; https://doi.org/10.1016/j.tifs.2019.04.003

[3] Wang, Laili, Xuemei Ding, and Xiongying Wu, Water science and technology 68, no. 11 (2013): 2485-2491; https://doi.org/10.2166/wst.2013.532

[4] Wang, Jie, Manglai Gao, Tao Shen, Mingming Yu, Yang Xiang, and Jian Liu, Journal of hazardous materials 366 (2019): 501-511; https://doi.org/10.1016/j.jhazmat.2018.12.031

[5] Bagheri, Samira, Amin TermehYousefi, and Trong-On Do, Catalysis Science & Technology 7, no. 20 (2017): 4548-4569; https://doi.org/10.1039/C7CY00468K

[6] Arul S, Senthilnathan T, Jeevanantham V, Satheesh Kumar KV, Archives of Metallurgy and Materials 66 (4), 1141-1148 https://doi.org/10.24425/amm.2021.136434

[7] Cardoso, Inês MF, Rita MF Cardoso, and Joaquim CG Esteves da Silva, Nanomaterials 11, no. 8 (2021): 2045; https://doi.org/10.3390/nano11082045

[8] Schneider, Jenny, Masaya Matsuoka, Masato Takeuchi, Jinlong Zhang, Yu Horiuchi, Masakazu Anpo, and Detlef W. Bahnemann, Chemical reviews 114, no. 19 (2014): 9919-9986; https://doi.org/10.1021/cr5001892

[9] Jeevanantham V, Tamilselvi D, Rathidevi K and Bavaji SR, P Neelakandan, Biomass Conversion and Biorefinery, 1-10, https://doi.org/10.1007/s13399-023-04179-9

[10] Feng, Hao-peng, Lin Tang, Guang-ming Zeng, Yaoyu Zhou, Yao-cheng Deng, Xiaoya Ren, Biao Song, Chao Liang, Meng-yun Wei, and Jiang-fang Yu, Advances in Colloid and Interface Science 267 (2019): 26-46; https://doi.org/10.1016/j.cis.2019.03.001

[11] Hastir, Anita, Nipin Kohli, and Ravi Chand Singh, Journal of Physics and Chemistry of Solids 105 (2017): 23-34; https://doi.org/10.1016/j.jpcs.2017.02.004

[12] Guan, Shengnan, Wenzhi Li, Jianru Ma, Yanyan Lei, Yuanshuai Zhu, Qifu Huang, and Xiaomeng Dou, Journal of Industrial and Engineering Chemistry 66 (2018): 126-140; https://doi.org/10.1016/j.jiec.2018.05.023

[13] Naseri, Neda, Hadi Valizadeh, and Parvin Zakeri-Milani, Advanced pharmaceutical bulletin 5, no. 3 (2015): 305; https://doi.org/10.15171%2Fapb.2015.043.
[14] Zheng, Lei, Fashui Hong, Shipeng Lu, and Chao Liu, Biological trace element research 104 (2005): 83-91; https://doi.org/10.1385/BTER:104:1:083
[15] Xiao, Deli, Ting Lu, Rong Zeng, and Yanping Bi, Microchimica Acta 183 (2016): 2655-2675; https://doi.org/10.1007/s00604-016-1928-y
[16] Jeevanantham V, Tamilselvi D, Bavaji SR and Mohan S, Bulletin of Materials Science, 46 (1), 32 (2023); https://doi.org/10.1007/s12034-022-02868-1
[17] Wang, Dongrui, Yaokang Zhang, Xi Lu, Zhijun Ma, Chuan Xie, and Zijian Zheng, Chemical Society Reviews 47, no. 12 (2018): 4611-4641; https://doi.org/10.1039/C7CS00192D
[18] Ahmed, Syed Nabeel, and Waseem Haider, Nanotechnology 29, no. 34 (2018): 342001; https://doi.org/10.1088/1361-6528/aac6ea
[19] Jeevanantham V, Tamilselvi D, Rathidevi K and Bavaji SR, Journal of Materials Research 38 (7), 1909-1918 https://doi.org/10.1557/s43578-023-00965-3